Journal of Power Sources 195 (2010) 2488–2495

Contents lists available at ScienceDirect

Journal of Power Sources

journal homepage: www.elsevier.com/locate/jpowsour

Hydrothermal preparation and electrochemical properties of Gd^{3+} and Bi^{3+}, Sm^{3+}, La^{3+}, and Nd^{3+} codoped ceria-based electrolytes for intermediate temperature-solid oxide fuel cell

Sibel Dikmen [a,*], Hasan Aslanbay [a], Erdal Dikmen [b], Osman Şahin [c]

[a] Department of Chemistry, Süleyman Demirel University, SDU, Fen-Edebiyat Fakultesi, Kimya Bolumu, 32260 Isparta, Turkey
[b] Department of Physics, Süleyman Demirel University, 32260 Isparta, Turkey
[c] Department of Physics, Mustafa Kemal University, Hatay, Turkey

ARTICLE INFO

Article history:
Received 28 April 2009
Received in revised form 27 October 2009
Accepted 18 November 2009
Available online 26 November 2009

Keywords:
SOFC
Hydrothermal preparation
Co-doping

ABSTRACT

The structure, the thermal expansion coefficient, electrical conductivities of $Ce_{0.8}Gd_{0.2-x}M_xO_{2-\delta}$ (for M: Bi, $x = 0$–0.1, and for M: Sm, La, and Nd, $x = 0.02$) solid solutions, prepared for the first time hydrothermally, are investigated. The uniformly small particle size (28–59 nm) of the materials allows sintering of the samples into highly dense ceramic pellets at 1300–1400 °C. The maximum conductivity, $\sigma_{700\,^\circ C}$ around 4.46×10^{-2} S cm^{-1} with $E_a = 0.52$ eV, is found at $x = 0.1$ for Bi-co-doping. Among various metal-co-dopings, for $x = 0.02$, the maximum conductivity, $\sigma_{700\,^\circ C}$ around 2.88×10^{-2} S cm^{-1} with $E_a = 0.67$ eV, is found for Sm-co-doping. The electrolytic domain boundary (EDB) of $Ce_{0.8}Gd_{0.1}Bi_{0.1}O_{2-\delta}$ is found to be 1.2×10^{-19} atm, which is relatively lower than that of the singly doped samples. The thermal expansion coefficients, determined from high-temperature X-ray data are 11.6×10^{-6} K^{-1} for the CeO_2, 12.1×10^{-6} K^{-1} for $Ce_{0.8}Gd_{0.2}O_{2-\delta}$, and increase with co-doping to 14.2×10^{-6} K^{-1} for $Ce_{0.8}Gd_{0.18}Bi_{0.02}O_{2-\delta}$. The maximum power densities for the single cell based on the codoped samples are higher than that of the singly doped sample. These results suggest that co-doping can further improve the electrical performance of ceria-based electrolytes.

1. Introduction

Solid oxide fuel cells (SOFCs) are important technologies for the power generation due to their environmentally friendly nature, high efficiency and fuel flexibility.

Electrolytes used for fuel cells are usually the main components determining the performance of the cell. A typical solid oxide fuel cell uses a high oxide ion conductor, 8 mol% yttria-stabilized zirconia (YSZ), as a solid electrolyte due to its thermal and mechanical strength. The use of YSZ requires to operate at high temperatures (800–1000 °C) to provide high level of ionic conductivity. However, operating at such high temperatures causes many problems; high fabrication cost, reaction between the cell components, and thermal expansion mismatch [1]. To reduce the operation temperature of the SOFC system, much attention has been paid by scientific community to investigate alternative electrolyte materials, e.g., Bi_2O_3- [2–4] and CeO_2- [5] based materials to increase the efficiency of the electrochemical device and decrease the application temperature. Although Bi_2O_3-based materials have significantly higher ionic conductivity compared to yttria-stabilized zirconia, their application as fuel cell electrolytes is hindered by their limited electrolytic domain [2]. The doped ceria has been considered to be a better candidate for use as an electrolyte in SOFCs in addition to its application in oxygen sensors, oxygen separations, etc. due to its higher oxide ion conductivity at much lower temperatures compared to YSZ [5,6].

Pure CeO_2 is a poor ionic conductor and has the fluorite structure with oxygen vacancies ($V_o^{\bullet\bullet}$) as the predominant ionic defect. So far, ceria-based electrolytes have been extensively studied and made much progress. Some singly doped electrolytes, such as $Ce_{1-x}Gd_xO_{2-\delta}$ (GDC), $Ce_{1-x}Sm_xO_{2-\delta}$ (SDC), $Ce_{1-x}Y_xO_{2-\delta}$ (YDC), etc., show high oxide ion conductivity at intermediate temperatures (500–700 °C) [5–10]. Substitution of the Ce^{4+} cations by a lower-valent metal ion (e.g., M^{3+}) in the lattice results in the oxygen vacancy formation and increases the ionic conductivity.

$$2CeO_2 \xrightarrow{2MO_{1.5}} 2M'_{Ce} + V_O^{\bullet\bullet} + 3O_O^x \quad (1)$$

The substitution of Ce^{4+} ($r_i = 0.111$ nm) by larger cations such as Gd^{3+} ($r_i = 0.119$ nm [11]) has been examined in great detail by a number of authors, and gadolinium-doped ceria is considered for being one of the best ceria-based solid electrolytes currently available [12].

* Corresponding author. Tel.: +90 246 2114164; fax: +90 246 2371106.
E-mail address: sdikmen@fef.sdu.edu.tr (S. Dikmen).

0378-7753/$ – see front matter © 2009 Elsevier B.V. All rights reserved.
doi:10.1016/j.jpowsour.2009.11.077

However, SOFCs based on these materials have not met the commercial requirement yet. One of the most important requirements for commercialization is the cost effectiveness of the cell components; therefore, the preparation and sintering temperature plays a major role on that.

In the past, many investigations have been carried out on various aspects of doped ceria solid electrolytes mostly prepared by conventional ceramic methods. As well known, the conventional ceramic methods usually require high preparation temperature, which is one of the reasons for its high cost. The sintering temperature for ceria-based ceramics varies from 1500 to 1700 °C, depending on the dopant, the particle size of the starting materials, preparation and sintering method. It is well known that ceria-based materials prepared by conventional ceramic methods are hard to densify below 1500 °C. Lowering sintering temperature for solid electrolyte makes the process to be cost effective since co-firing with the anode and cathode materials is possible. Operating at low temperatures also enables the use of inexpensive materials as interconnects, and enhances the stability and durability of all the components. Various rare-earth doped ceria have successfully been obtained by hydrothermal treatment, providing low-temperature preparation and morphological control of ultrafine particles of uniform crystallite dimension. Ceramics prepared by hydrothermal treatment generally require lower sintering temperatures to achieve the same degree of densification than the ones prepared by conventional solid-state ceramic methods [13–17].

On the other hand, the ceria-based electrolytes easily develop n-type electronic conduction when exposed to the reducing atmosphere of the fuel cell anode, which causes the efficiency loss. It is therefore important to make efforts towards the reduction of electronic conductivity. The electrolytic domain boundary (EDB) is an important property of mixed (ionic and electronic) conductors, which separates the ionically and electronically conducting regions. It is actually defined as the oxygen partial pressure at which the electronic conductivity is equal to the ionic conductivity. The lower the EDB, the wider the electrolytic domain. Effect of codoping on electrical conductivity has been investigated [18–22]. Guang et al. reported that yttrium–gadolinium-codoped ceria has lower electrolytic domain boundary compared to that of singly doped ceria [18].

In the current research, with the aim to develop new ceria-based electrolyte materials with improved electrochemical properties, Gd^{3+} and M^{3+} ($M = Bi^{3+}$, Sm^{3+}, La^{3+}, and Nd^{3+}) codoped ceria materials were prepared for the first time hydrothermally to the best of our knowledge. We present the results of a systematic study of the structure, electrical and thermophysical properties of the materials mentioned above and the comparison of the results of codoped materials with singly doped ones.

2. Experimental

A series of solid solutions with the general formula of $Ce_{0.8}Gd_{0.2-x}M_xO_{2-\delta}$ (for M: Bi, $x = 0$, 0.01, 0.02, 0.03, 0.04, 0.05, and 0.1, and for M: Sm, La, and Nd, $x = 0.02$) were synthesized by the hydrothermal method as previously reported for the Bi-, La-, and Gd-singly doped ceria solid electrolytes [15–17]. The stoichiometric amounts of cerium(III) nitrate hexahydrate ($(Ce(NO_3)_3 6H_2O)$, 99.99% Aldrich), gadalinium(III) nitrate hexahydrate ($(Gd(NO_3)_3 6H_2O)$, 99.9%, Aldrich), bismuth(III) nitrate hexahydrate ($Bi(NO_3)_3 6H_2O$), 99.9%, samarium(III) nitrate hexahydrate ($Sm(NO_3)_3 6H_2O$), 99.9%, lanthanum(III) nitrate hexahydrate ($(La(NO_3)_3 6H_2O)$, 99.9%, Aldrich), and neodymium(III) nitrate hexahydrate ($(Nd(NO_3)_3 6H_2O)$, 99.9%, Aldrich) were dissolved separately in water, mixed and co-precipitated with ammonium hydroxide at pH 10. The precipitated gels were sealed into teflon-lined steel autoclaves and hydrothermally treated at 260 °C for 12 h. The autoclaves were quenched at 260 °C to room temperature and crystallized powder of $Ce_{0.8}Gd_{0.2-x}M_xO_{2-\delta}$ (M: Bi, Sm, La, and Nd, and $x = 0$, 0.01, 0.02, 0.03, 0.04, 0.05, and 0.1) solid solutions were repeatedly washed with deionized water and dried in air at room temperature (Fig. 1).

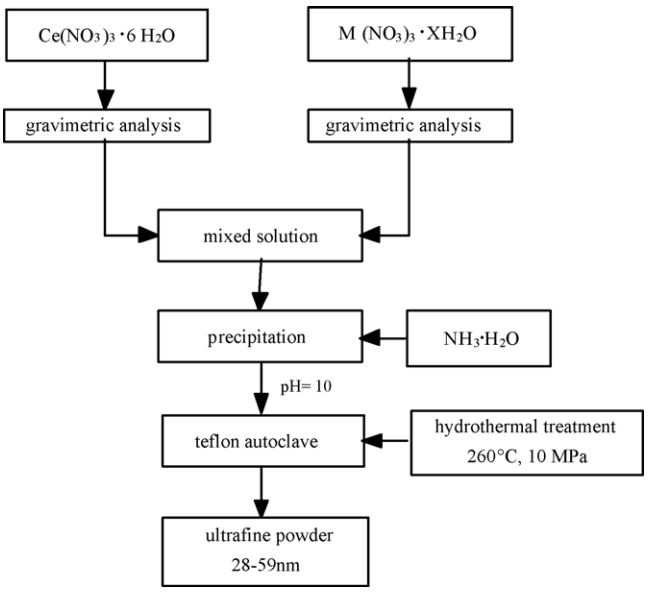

Fig. 1. Flow diagram of the hydrothermal synthesis.

Thermogravimetric analysis (TGA) measurements were carried out in the temperature range of 25–800 °C with TGA 2050 with a heating and cooling rate of 1 °C min^{-1} to determine the exact stoichiometry of hydrates before starting the sample preparation.

The room temperature powder X-ray diffraction patterns (PXD) of the ultra fine powders were obtained with a Rigaku D/Max-2200/PC diffractometer with monochromatized Cu Kα radiation at a 2θ scan of 1° min^{-1}. Cell parameters were calculated by fitting the observed reflections with a least-squares program. The reflection from the (1 1 1) plane was used for the determination of the average crystallite size, D, of the hydrothermally prepared powders calculated from the Scherrer formula:

$$D = \frac{0.9\lambda}{\beta \cos\theta} \quad (2)$$

where λ is the wavelength of the X-rays, θ is the diffraction angle, $\beta = \sqrt{(\beta_m^2 - \beta_s^2)}$ is the corrected halfwidth of the observed halfwidth, β_m, of the (1 1 1) reflection in samples of $Ce_{0.8}Gd_{0.2-x}M_xO_{2-\delta}$ (for M: Bi, $x = 0$, 0.01, 0.02, 0.03, 0.04, 0.05, and 0.1, and for M: Sm, La, and Nd, and $x = 0.02$) and β_s is the halfwidth of the (1 1 1) reflection in a standard sample of CeO_2 ($D \sim 100$ nm).

The dried powders were ground in an agate mortar and then pressed under a pressure of about 200 MPa into cylindrical pellets (11.3 mm in diameter and 0.7–1 mm in thickness). The pellets were sintered at 1350 °C in air for 5 h with a program heating and cooling rate of 2 °C min^{-1}.

The density of the sintered samples was measured both by employing Archimedes principle, and by measuring the dimensions method. It was found that almost the same values for the densities were obtained by the two methods used. The average value derived from the two methods for each specimen was then compared to the theoretical one, calculated from the lattice parameters. The sintered samples were more than the 95–97% of the theoretical density in all cases.

To examine the surfaces, investigations were performed by JEOL JSM-5400 scanning electron microscope (SEM). For SEM exami-

nations, the samples were coated with a gold thin layer to avoid charging effects.

The thermal stability of the materials was checked by means of PXD patterns of the samples heated at 800 and 1000 °C for 2 weeks.

The thermal expansion coefficients of the samples were calculated by the lattice parameters as a function of the temperature obtained by high-temperature powder X-ray diffraction patterns (PXD) with a Rigaku D/Max-2200/PC diffractometer equipped with a high-temperature attachment with monochromatized Cu Kα radiation at a 2θ scan of $1^\circ\,min^{-1}$.

Impedance spectroscopy allows for easy determination of the total conductivity and, at low temperatures (<500 °C), the bulk (intragranular, high frequency) and the grain boundaries (intergranular, intermediate frequency) contribute to the total conductivity. The electrical conductivity of the materials was measured on a sintered ceramic pellet. Silver paste was painted onto two faces of the pellets, using Alfa paste. The sample was then dried and fired at 500 °C for 1 h with a heating and cooling rate of $5\,^\circ C\,min^{-1}$. The reason for choosing the silver electrodes over platinum electrodes was that the silver electrodes exhibited a smaller resistivity than platinum electrodes and also at high temperatures, the resistance of the platinum electrodes was seen to increase by the increased time spent. The AC impedance measurements were carried out via a two probe method using a homemade quartz sample holder with platinum wires as current collectors on three different sets of pellets of each composition. Solartron 1260 A Frequency Response Analyzer was used to carry out the measurements at frequencies ranging from 0.01 Hz to 10 MHz on isothermal plateaus 30 min long, in air on heating every 25 °C up to 700 °C (and 700 down to 150 °C). Data were collected with SMART program and fitted to the corresponding equivalent circuits with the program ZView. The resistance of the wires in the sample holder at temperatures more than 500 °C was measured and subtracted from the total measured resistance. The total resistance of electrolyte is given by

$$R_t = R_b + R_{gb} \tag{3}$$

where R_t, R_b and R_{gb} represent total resistance, bulk resistance and grain boundary resistance, respectively.

Then the conductivity can be calculated using the equation:

$$\sigma = \frac{L}{SR} \tag{4}$$

where L and S stand for the sample thickness and the electrode area of the sample surface, respectively. 4-Point DC method was also employed to obtain the total conductivity of the prepared samples.

In order to determine the oxide ion transference numbers, the EMF of the following oxygen concentration cell was measured:

$$O_2,\ p(O_2)a,\ Ag|Ce_{0.8}Gd_{0.2-x}MxO_{2-\delta}|Ag,\ p(O_2)c,\ O_2 \tag{5}$$

If the conduction in ceria solid solutions is predominantly ionic, the theoretical EMF (E_{th}) is given by the Nernst equation:

$$E_{th} = \frac{RT}{4F}\ \ln\frac{p(O_2)a}{p(O_2)^c}, \tag{6}$$

where R, T, and F are the gas constant, the temperature and the Faraday constant, respectively, and $p(O_2)a = 1.01 \times 10^5$ and $p(O_2)c = 0.21 \times 10^5$ Pa are oxygen partial pressures at the anode (pure oxygen) and cathode (air), respectively. If the specimen has some electronic conduction, the measured EMF, E, will be lower than E_{th} because of the discharge of the electrochemical cell due to the electronic conduction. If the electrodes are sufficiently reversible, the oxide ion transference numbers, t_i can be calculated as follows:

$$t_i = \frac{\sigma_i}{\sigma_i + \sigma_e} = \frac{E}{E_{th}} \tag{7}$$

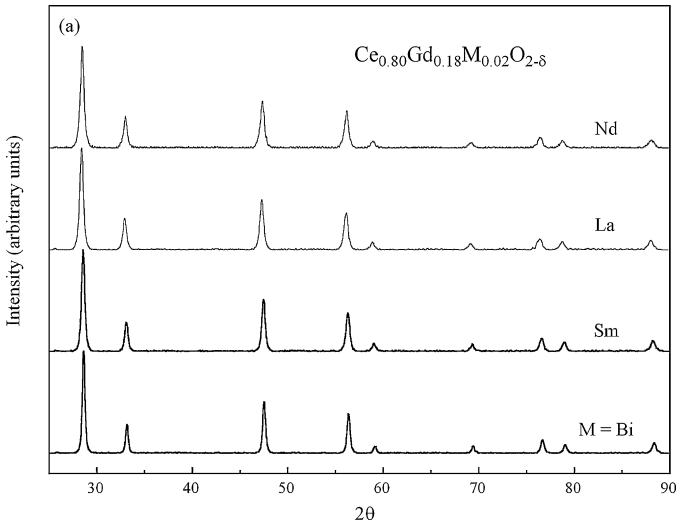

Fig. 2. Powder X-ray diffraction patterns of $Ce_{0.8}Gd_{0.18}M_{0.02}O_{2-\delta}$ solid solutions.

where σ_i and σ_e are ionic and electronic conductivities, respectively.

4-Point DC method was employed to obtain the total conductivity as a function of oxygen partial pressures on rectangular samples. The oxygen partial pressure was adjusted by changing the mixing ratio of oxygen, hydrogen, argon and water vapor with digital mass flow controllers (Aera FC-D980C). O_2 + Ar was used for oxidizing conditions, $P_{O_2} = 0.21$ atm. Reducing conditions ($P_{O_2} = 10^{-25}$ to 10^{-14}) were obtained by varying H_2, Ar and water vapor mixing ratios. Flow rate of these mixture gases was $100\,cm^3\,min^{-1}$. A yttria-stabilized zirconia-based high-temperature oxygen sensor was used to measure the oxygen partial pressure in situ. The electrolytic domain boundaries was taken as the P_{O_2} at which the ionic conductivity equals the electronic conductivity.

Single cells were constructed based on the electrolyte pellets. An anode of NiO (70 wt.%-GBDC (gadolinium–bismuth-codoped ceria)) cermet was mixed with terpineol and ethyl cellulose to form a slurry, subsequently painted on one side of GBDC electrolyte as the anode, which was annealed at 1200 °C for 2 h. $La_{0.6}Sr_{1.4}MnO_{4+\delta}$ which was prepared by a method described else where [23], were mixed with terpineol and ethyl cellulose to form a slurry, then slurry was painted on the other side of the GBDC electrolyte as the cathode, and the whole was first heated at 400 °C for 2 h to remove organic binders, and then sintered at 950 °C for 4 h in air with a heating and cooling rate of $2\,^\circ C\,min^{-1}$. The platinum meshes and wires were attached to both cathode and anode as leaders with Alfa silver paste. The cell was then sealed in a specially designed quartz tube with a sealant (Aremco Ceramabond™ 552 High Temperature Ceramic Adhesives & Pastes). The fuel cell test was performed by two electrode method using a Keithley 2400 digital source meter from 600 to 800 °C. H_2 with 3% H_2O and air were used as fuel and oxidant gases, respectively.

3. Results and discussion

Fig. 2 shows the X-ray diffraction patterns of the $Ce_{0.8}Gd_{0.18}M_{0.02}O_{2-\delta}$ solid solutions prepared hydrothermally. It can be seen that all crystallite powders are single phase with cubic fluorite structure. The PXD data in Fig. 3 show that $Ce_{0.8}Gd_{0.2-x}Bi_xO_{2-\delta}$, prepared by hydrothermal method, forms solid solutions with the fluorite structure in the Bi substitution range of $x = 0$–0.1. It can be seen from Fig. 3, that the introduction of Bi_2O_3 into gadolinium-doped ceria can cause a small shift to the right in the ceria peaks, which is indicative of change in lattice

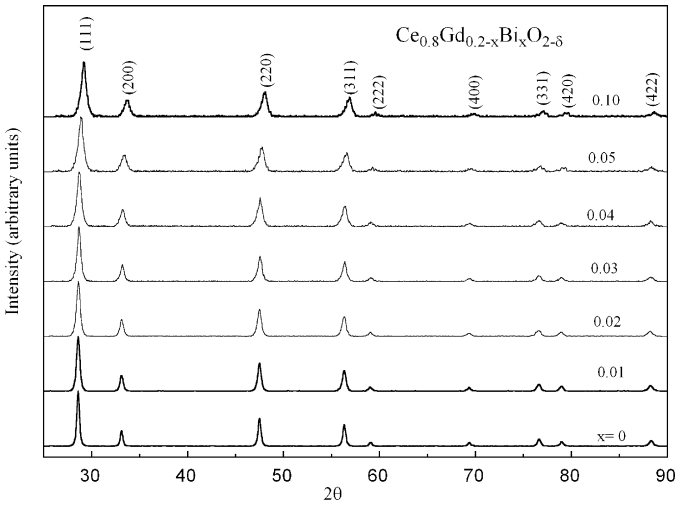

Fig. 3. Powder X-ray diffraction patterns of $Ce_{0.8}Gd_{0.2-x}Bi_xO_{2-\delta}$ solid solutions.

parameters. The fluorite phase evolution of $Ce_{0.8}Gd_{0.18}Bi_{0.02}O_{2-\delta}$ in the hydrothermal process as a function of heat-treatment time at 260 °C was examined by PXD. After 30 min heating, the precipitated product is a fine crystalline powder (~10–15 nm average particle size) of gadolinium–bismuth-codoped solid solution (Fig. 4). Further hydrothermal heat-treatment increases the crystallinity of the powder: e.g., 22 nm in 60 min, 32–36 nm in 90 min, and ~54 nm in 12 h. The unit cell parameter a is higher than that of the pure CeO_2 for all substitution range, which is in good agreement with effective ionic radii of Ce^{4+} (0.111 nm), Gd^{3+} (0.119 nm), and Bi^{3+} (0.131 nm). Bi_2O_3 doping into CeO_2 lattice will cause elastic deformation of the material and therefore induce uniform strain in the lattice causing the diffraction peaks to shift to new 2θ positions. As can be seen from Fig. 5 that the lattice parameters decrease linearly as Bi content increases (Table 1). The similar results were reported earlier by Fu et al. [24] for $Ce_{0.8}(Gd_{1-x}Bi_x)_{0.2}O_{1.9}$ ceramics prepared by co-precipitation method for $x = 0.1$–0.5.

The thermal stability of the solid solution $Ce_{0.8}Gd_{0.18}Bi_{0.02}O_{2-\delta}$ annealed at 800 and 1000 °C for 2 weeks was shown by means of PXD in Fig. 6. It can be seen from Fig. 6 that, this composition is

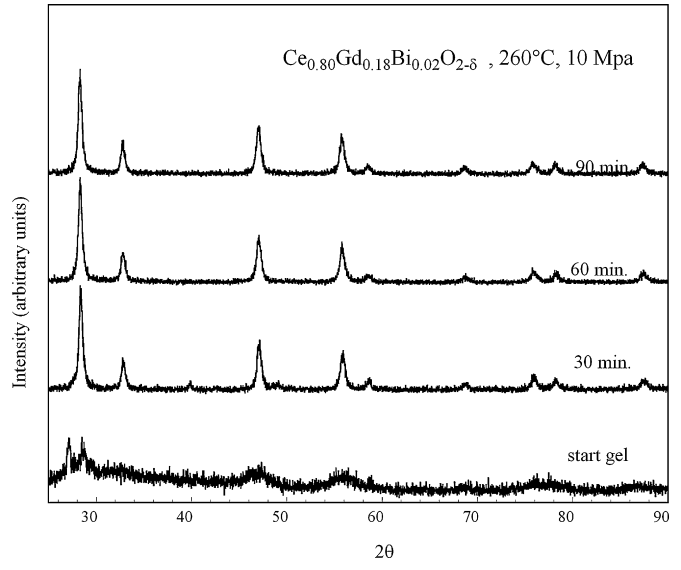

Fig. 4. Evolution of the powder X-ray diffraction patterns of the $Ce_{0.8}Gd_{0.18}Bi_{0.02}O_{2-\delta}$ solid solution, as a function of time at 260 °C during hydrothermal preparation.

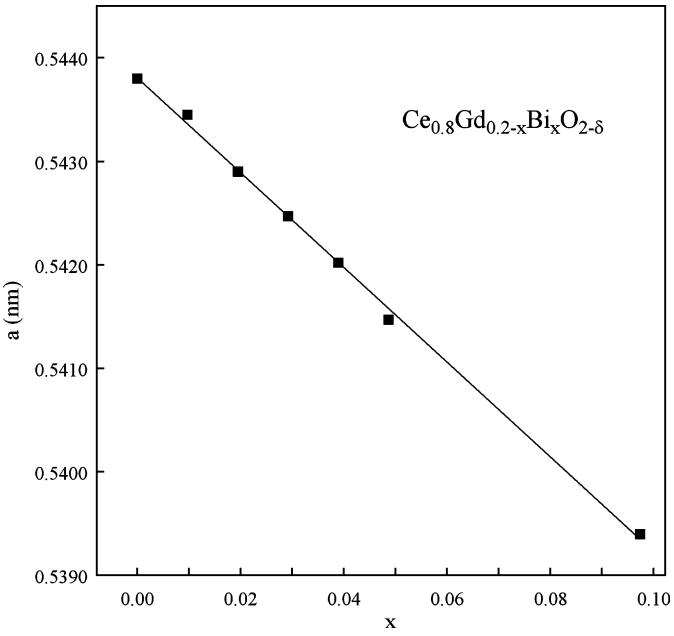

Fig. 5. Lattice constants of $Ce_{0.8}Gd_{0.2-x}Bi_xO_{2-\delta}$ solid solutions as a function of x.

Table 1
Lattice parameters, crystallite sizes of hydrothermally prepared $Ce_{0.8}Gd_{0.2-x}Bi_xO_{2-\delta}$ solid solutions.

Composition	Lattice parameter a (nm)	Average crystallite size, D (nm)
$x = 0$	0.54380	65
$x = 0.01$	0.54345	59
$x = 0.02$	0.54290	48
$x = 0.03$	0.54247	36
$x = 0.04$	0.54202	33
$x = 0.05$	0.54147	31
$x = 0.10$	0.53940	28

thermally stable at 800 and 1000 °C even after 2 weeks annealing at these temperatures. Singly doped Gd sample on the other hand was decomposed at 1000 °C after a week annealing [19]. The average crystallite size, D, of Gd- and Bi-codoped ceria powders, calculated by the Scherrer Formula from PXD data were between 18 and 37 nm (Table 1). Temperature dependent X-ray diffraction measurements clearly show that the lattice parameter a increases with temperature (Fig. 7); the thermal expansion coefficient deter-

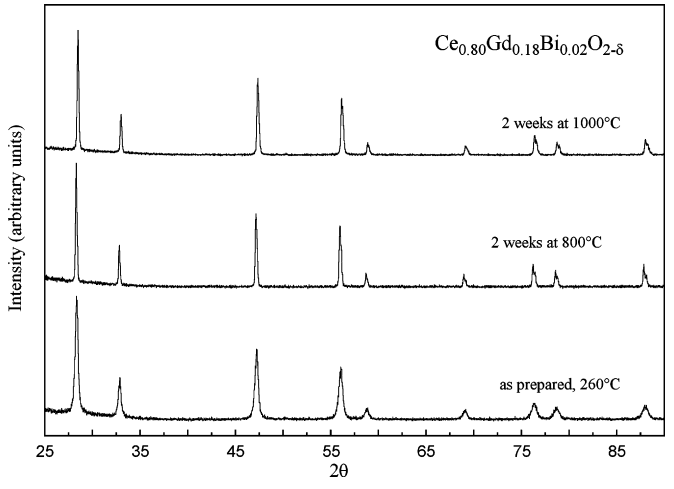

Fig. 6. Powder X-ray diffraction patterns of the $Ce_{0.8}Gd_{0.18}Bi_{0.02}O_{2-\delta}$ solid solution after annealing for 2 weeks at 800–1000 °C.

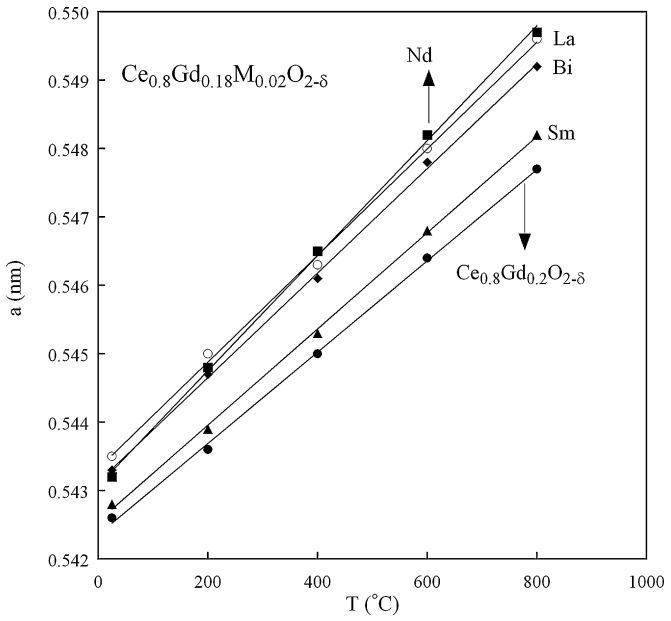

Fig. 7. Temperature dependence of the lattice parameters of $Ce_{0.8}Gd_{0.18}M_{0.02}O_{2-\delta}$ (M: Bi, Sm, La, and Nd) solid solutions.

Table 2
Thermal expansion coefficient of $Ce_{0.8}Gd_{0.18}M_{0.02}O_{2-\delta}$ solid solutions.

M	TEC ($\times 10^{-6}$ K^{-1})
Bi	14.2
Sm	12.8
La	14.5
Nd	15.4

mined from the data of Fig. 7 is 11.7×10^{-6} K^{-1} for pure CeO_2, and, increase with Gd- and M-codoping as presented in Table 2.

The fine substituted ceria powders were sintered into pellets at 1300–1400 °C with apparent densities of more than 95% of the theoretical value while ceria solid electrolytes, prepared by conventional ceramic techniques require more than 1600 °C to get this density. In Fig. 8, the SEM micrograph of the ceria solid solution $Ce_{0.8}Gd_{0.18}Bi_{0.02}O_{2-\delta}$ sintered at 1350 °C indicates relatively small particles of uniform size, 1 μm, and very dense microstructure. As expected, these particles are considerably larger than those of the 'as-prepared' powder (~40 nm).

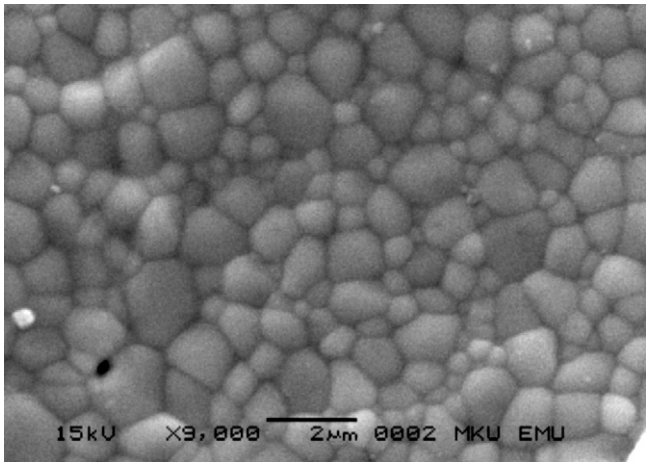

Fig. 8. Scanning electron micrograph of the surface of $Ce_{0.8}Gd_{0.18}Bi_{0.02}O_{2-\delta}$ densified at 1350 °C.

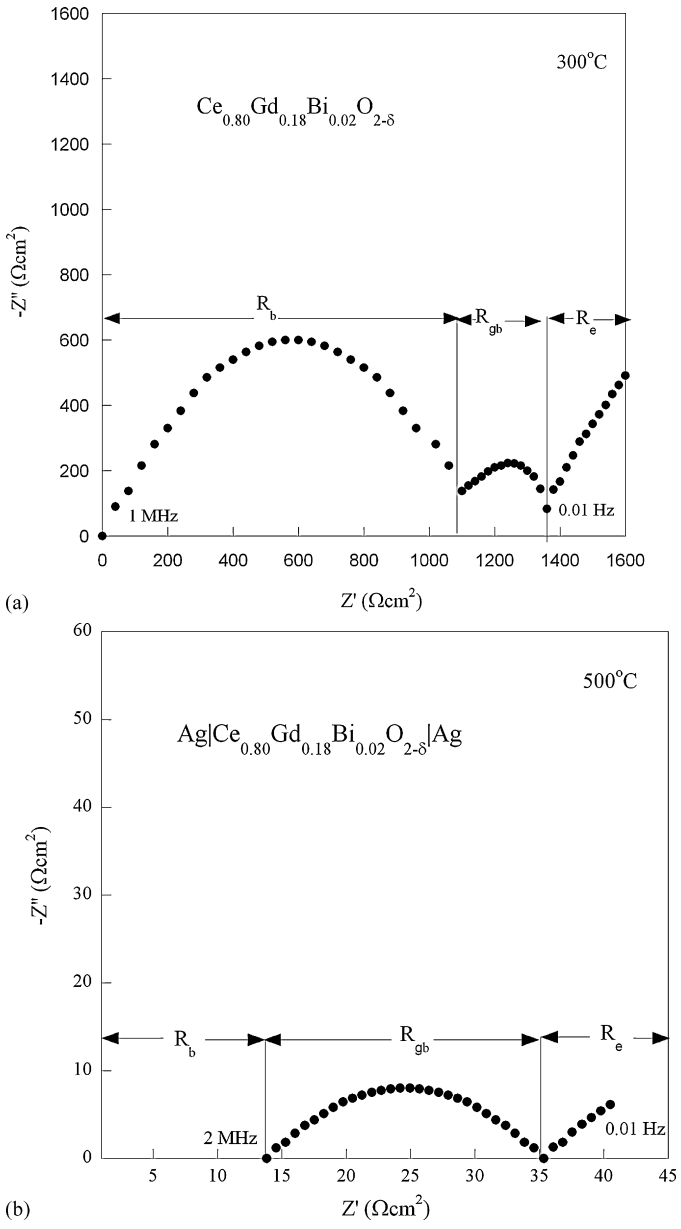

Fig. 9. The complex impedance plots for the cell, air, Ag| $Ce_{0.8}Gd_{0.18}Bi_{0.02}O_{2-\delta}$ |Ag, air (a) at 300 °C, and (b) at 500 °C.

AC impedance plots of $Ce_{0.8}Gd_{0.18}Bi_{0.02}O_{2-\delta}$ specimen obtained at two temperatures (300 and 500 °C) are shown in Fig. 9(a) and (b). These temperatures represent two extremes, and it can be seen that the semicircles appearances and their intersections with real axis (Z') change with the temperature of the measurements. The semicircle corresponding to the bulk conductivity can easily be seen in Fig. 9(a) at 300 °C. At higher temperatures, the time constant associated with bulk impedances decreases, therefore, around ~500 °C, the bulk semicircle disappears. Pure ceria oxide is basically a poor oxide ion conductor ($\sigma_{700\,^\circ C} \sim 10^{-4}$ S cm^{-1}). The ionic conductivities are significantly enhanced in $Ce_{0.8}Gd_{0.2-x}Bi_xO_{2-\delta}$ solid electrolytes by increasing the oxygen vacancies ($V_O^{\bullet\bullet}$). The Arrhenius plot for the electrical conductivity of $Ce_{0.8}Gd_{0.2-x}Bi_xO_{2-\delta}$ solid solutions is plotted in Fig. 10. Similar to the previously reported systems [13–17], the electrical conductivity of $Ce_{0.8}Gd_{1-x}Bi_xO_{2-\delta}$ increases systematically with increasing bismuth substitution and reaches a maximum for the composition $Ce_{0.8}Gd_{0.1}Bi_{0.1}O_{2-\delta}$ ($\sigma_{700\,^\circ C} \sim 4.46 \times 10^{-2}$ S cm^{-1}).

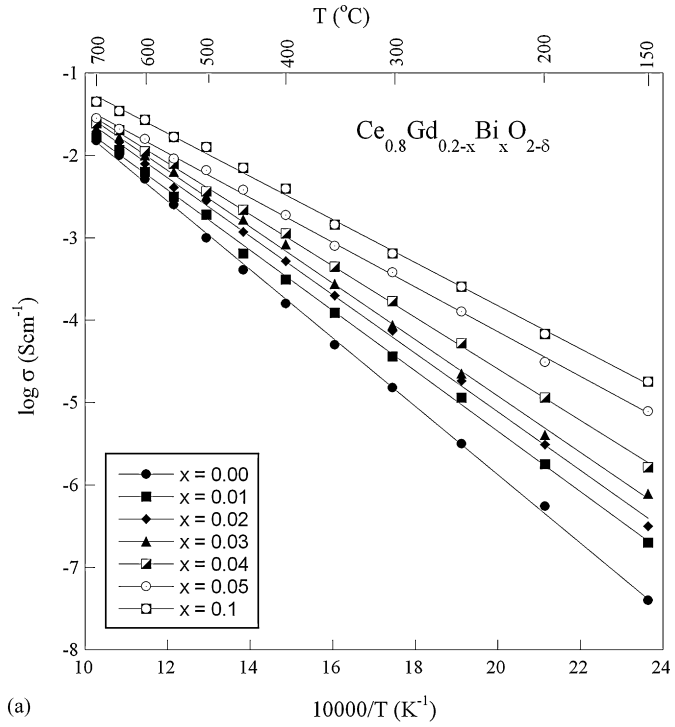

(a)

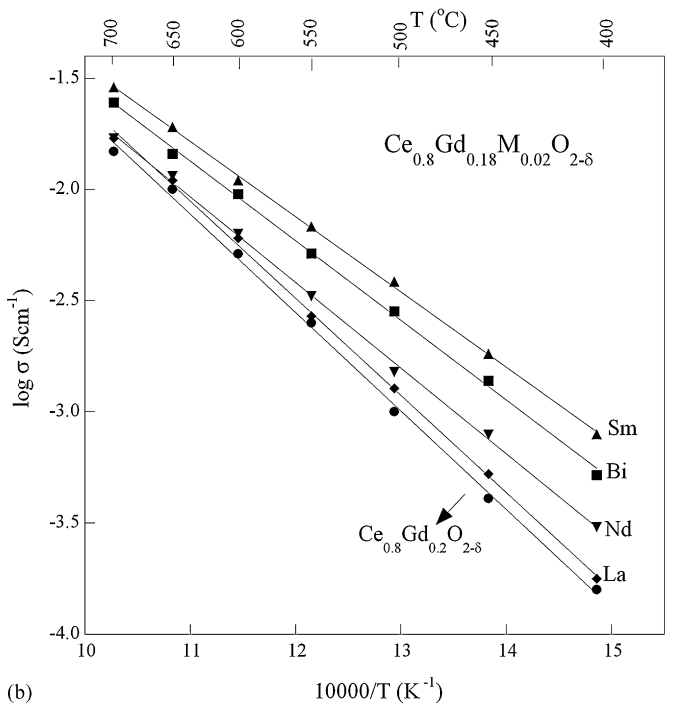

(b)

Fig. 10. Arrhenius plots of the ionic conductivity of (a) $Ce_{0.8}Gd_{0.2-x}Bi_xO_{2-\delta}$, and (b) $Ce_{0.8}Gd_{0.18}M_{0.02}O_{2-\delta}$ solid solutions.

With increasing temperature the oxide ion mobility increases, and the conductivities approach the similar values at high temperatures. The activation energy decreases with increasing Gd and Bi substitution and reaches to the lowest value for the composition $Ce_{0.8}Gd_{0.1}Bi_{0.1}O_{2-\delta}$ (E_a = 0.52 eV), due to the weaker Gd^{3+}–O and Bi^{3+}–O bond compared to that of Ce^{4+}–O. The migration enthalpy (ΔH_m) for oxide anions through the ceria lattice is dependent upon both the oxygen binding energy in the lattice and the 'free volume' through which the oxide ions migrate, i.e. ΔH_m is the sum of the energy required to break a lattice cation-oxygen bond and

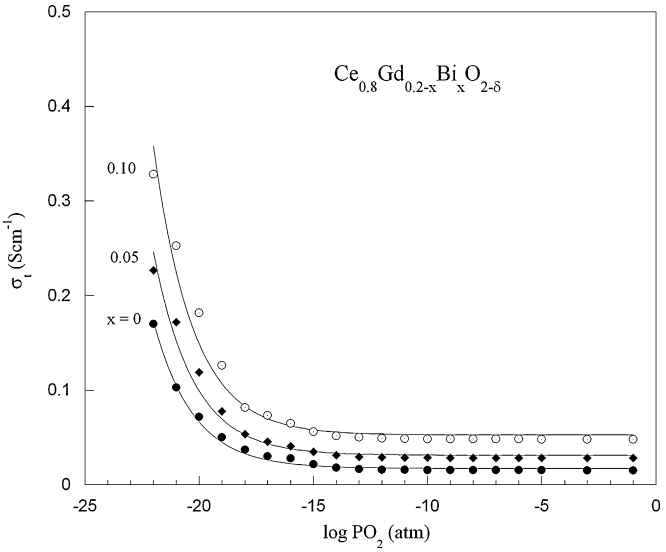

Fig. 11. Oxygen partial pressure dependence of the total conductivity of $Ce_{0.8}Gd_{0.2-x}Bi_xO_{2-\delta}$ solid solutions at 973 K. The data are fitted with $\sigma_t = \sigma_i + k\,P_{O_2}^{-1/4}$.

an energy term dependent on oxide ion mobility between vacant lattice sites. The average M–O binding energy (ABE) in the lattice, ABE = (1−x) BE(Ce–O) + xBE (Gd/Bi–O), decreases linearly with increasing Gd/Bi content. The 'free volume', defined as the difference between the ceria unit cell volume (as calculated from the unit cell parameters) and the total volume occupied by all the ions present within the unit cell (calculated from the effective ionic radii), tends to increase with increasing Gd and Bi substitutions. Fig. 10(b) shows the Arrhenius plot of $Ce_{0.8}Gd_{0.18}M_{0.02}O_{2-\delta}$ (M = Bi, Sm, La, and Nd), and as can be seen from figure, codoping with various metals mentioned above improved the ionic conductivity compared to the singly doped one. Among the various codoping substituents, the one with Sm gave the best results ($\sigma_{700\,^\circ C}(2.88\times10^{-2}\,S\,cm^{-1})$). These results prove that co-doping with an optimum ratio of gadolinium and the metals mentioned above can further improve the electrical property of ceria electrolytes.

The ionic transference number measurements with a concentration electrochemical cell have shown that the conductivity of all the investigated ceria samples is predominantly ionic (ti > 0.95).

The dependence of total conductivities of $Ce_{0.8}Gd_{0.2-x}Bi_xO_{2-\delta}$ (x = 0, 0.05, and 0.1 only for the sake of clarity) as a function of oxygen partial pressure has been shown in Fig. 11. As can be seen, the total electrical conductivity (σ_t) is predominantly ionic and remains constant at moderate P_{O_2}, whereas at low P_{O_2}, the total electrical conductivity increases as P_{O_2} decreases and is predominantly electronic. The electronic conductivity is proportional to $P_{O_2}^{-1/4}$. The data for EDB where the electronic conductivity equals to the ionic conductivity are listed in Table 4 for three different compositions. Results show that bismuth addition moved EDB to the lower oxygen partial pressure. Among various doped ceria samples, $Ce_{0.8}Gd_{0.1}Bi_{0.1}O_{2-\delta}$ has been shown to have better stability exhibiting the smallest EDB at lower oxygen partial pressures than the others. In Fig. 12, the dependence of electrical conductivity of $Ce_{0.8}Gd_{0.1}Bi_{0.1}O_{2-\delta}$ solid solution as a function of oxygen partial pressure has been shown for various temperatures, and EDB is listed in Table 3. As can be seen from the table, as the temperature decreases, the EDB moves to lower P_{O_2}. From these results, we can conclude that co-doping with Gd^{3+} and Bi^{3+} can lead to an improvement of the stability of ceria-based electrolytes at intermediate temperatures.

Table 3
Electrical conductivities, and activation energies of $Ce_{0.8}Gd_{0.2-x}Bi_xO_{2-\delta}$ solid solutions.

Composition	Electrical conductivity, σ (S cm^{-1})			Activation energy (eV)
	773 K	873 K	973 K	
$x=0$	1.03×10^{-3}	5.13×10^{-3}	1.51×10^{-2}	0.83
$x=0.01$	1.91×10^{-3}	6.31×10^{-3}	1.66×10^{-2}	0.74
$x=0.02$	2.83×10^{-3}	7.94×10^{-3}	1.95×10^{-2}	0.71
$x=0.03$	3.23×10^{-3}	1.02×10^{-2}	2.14×10^{-2}	0.67
$x=0.04$	3.66×10^{-3}	1.12×10^{-2}	2.45×10^{-2}	0.60
$x=0.05$	6.61×10^{-3}	1.58×10^{-2}	2.82×10^{-2}	0.56
$x=0.10$	1.26×10^{-2}	2.70×10^{-2}	4.46×10^{-2}	0.52

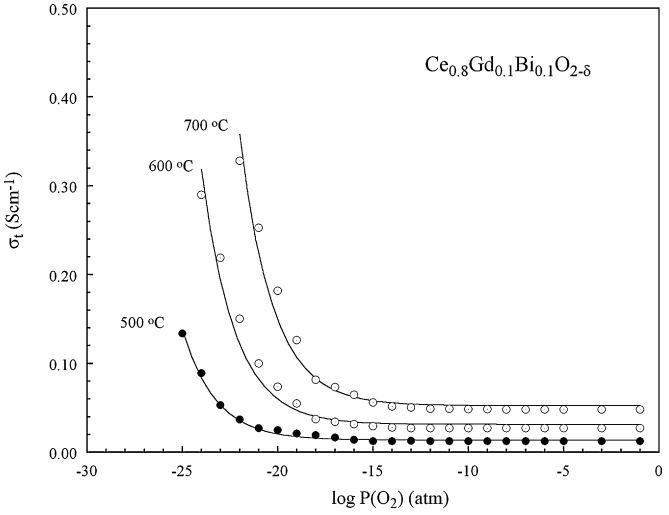

Fig. 12. Oxygen partial pressure dependence of the total conductivity of $Ce_{0.8}Gd_{0.1}Bi_{0.1}O_{2-\delta}$ at various temperatures. The data are fitted with $\sigma_t = \sigma_i + k\,P_{O_2}^{-1/4}$.

Fig. 13 shows *I–V* and *I–P* characteristics for various single cells with $Ce_{0.8}Gd_{0.2-x}Bi_xO_{2-\delta}$ solid solutions ($x=0$, 0.05, and 0.1) at the operating temperature of 700 °C. It is obvious that both the maximum current density and the maximum power density for the fuel cells using $Ce_{0.80}Gd_{0.15}Bi_{0.05}O_{2-\delta}$, and $Ce_{0.8}Gd_{0.1}Bi_{0.1}O_{2-\delta}$ electrolytes are higher than those of singly doped ceria with the same vacancy concentration. This is consistent with the electrical conductivity measurement results proving that codoping improved the electrochemical properties of singly doped ceria. Fig. 14 shows *I–V* and *I–P* characteristics for various single cells with

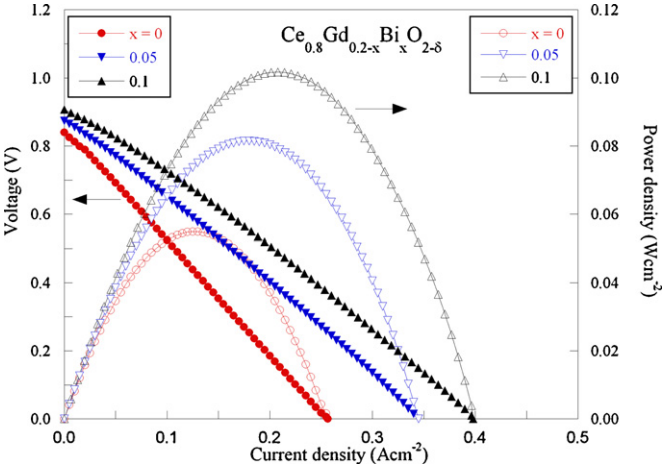

Fig. 13. Cell voltage and power density as a function of current density at 973 K for fuel cell using $Ce_{0.8}Gd_{0.2-x}Bi_xO_{2-\delta}$ electrolytes.

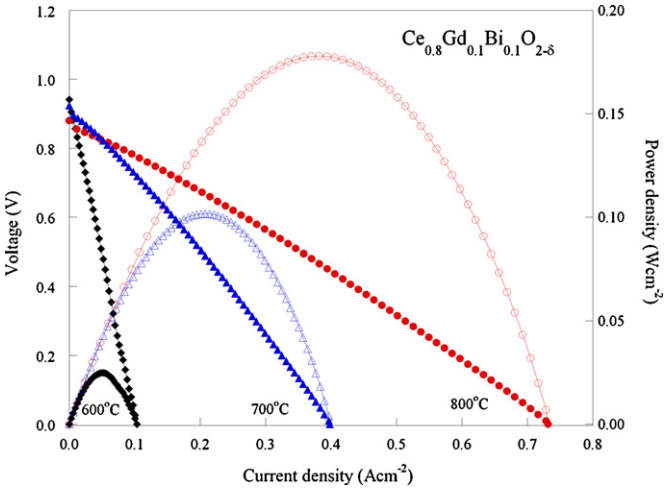

Fig. 14. Cell voltage and power density as a function of current density at various temperatures for fuel cell using $Ce_{0.8}Gd_{0.1}Bi_{0.1}O_{2-\delta}$ electrolyte.

Table 4
Electrolytic domain boundary (EDB) where the electronic conductivity equals to the ionic conductivity of $Ce_{0.8}Gd_{0.2-x}Bi_xO_{2-\delta}$ solid solutions.

Composition	Electrolytic domain boundary, EDB (atm)		
	973 K	873 K	773 K
$x=0$	6.53×10^{-19}		
$x=0.05$	2.29×10^{-19}		
$x=0.10$	1.20×10^{-19}	9.24×10^{-21}	6.76×10^{-22}

$Ce_{0.8}Gd_{0.1}Bi_{0.1}O_{2-\delta}$ solid solutions at the operating temperature of 700, 650, and 600 °C. It can be seen from the figure that open-circuit voltage (OCV) is 0.88 V at 800 °C, and increases to 0.94 V at 600 °C, which is close to its theoretical value. The small change in OCVs suggests that codoped sample is quite stable towards the Ce^{4+} reduction, keeping the ionic transference number high, at both temperatures. The maximum power densities were about 23, 102, and 178 mW cm^{-2} and the maximum current densities were about 104, 398, and 697 mA cm^{-2}, when the cell was operated at 600, 700, and 800 °C, respectively. The thickness of the electrolyte was ~1 mm, so, the cell performance of the cell can be considered encouraging. Much higher power densities would easily be obtained using a thin-film electrolyte (Table 4).

4. Conclusions

$Ce_{0.8}Gd_{0.2-x}M_xO_{2-\delta}$ (for M: Bi, $x=0$, 0.01, 0.02, 0.03, 0.04, 0.05, and 0.1, and for M: Sm, La, and Nd, $x=0.02$) solid solutions with the fluorite structure were prepared for the first time by a soft hydrothermal method at 260 °C and 10 MPa. Ultrafine particles of uniform crystallite dimension, ~18–37 nm can be formed in 30 min under hydrothermal conditions. Because of the small particle size of the ceria powder, the sinter-

ing temperature needed to obtain a dense ceramic pellet was reduced substantially from 1650 °C, that required for the ceria solid electrolytes prepared by conventional solid-state methods, to ~1300–1400 °C. The highest conductivity was found for $Ce_{0.8}Gd_{0.1}Bi_{0.1}O_{2-\delta}$ ($\sigma_{700\,^\circ C} \sim 4.46 \times 10^{-2}$ S cm^{-1}, $E_a = 0.52$ eV), which is predominantly ionic (ti > 0.95). Among various co-dopings for $x = 0.02$, the highest conductivity was found for samarium-codoped sample ($\sigma_{700\,^\circ C}(2.88 \times 10^{-2}$ S cm^{-1}, $E_a = 0.67$ eV)). The oxide ion conductivity is almost three times higher than that of the singly doped ceria for the same vacancy concentration ($Ce_{0.8}Gd_{0.2}O_{2-\delta}$, ($\sigma_{700\,^\circ C} \sim 1.51 \times 10^{-2}$ S cm^{-1}), $E_a = 0.83$ eV) and an order of magnitude higher than the most commonly used solid electrolyte, stabilized zirconia at corresponding temperatures ($\sigma_{700\,^\circ C}(\sim 10^{-3}$ S cm^{-1})). Electrolytic domain boundary was found to be lower, 1.2×10^{-19} atm for $Ce_{0.8}Gd_{0.1}Bi_{0.1}O_{2-\delta}$ compared to that of singly doped-electrolyte 6.53×10^{-19} atm, proving that the electrochemical properties are improved by co-doping. The maximum power density of the single cell using $Ce_{0.8}Gd_{0.1}Bi_{0.1}O_{2-\delta}$ electrolyte was found to be 102 mW cm^{-2}, which is higher than that of the singly doped sample, 54 mW cm^{-2} at 700 °C.

Acknowledgments

This work was funded by The Scientific and Technological Research Council of Turkey, under contrast no. TUBİTAK 106T536.

References

[1] H. Inaba, H. Tagawa, Solid State Ionics 83 (1996) 1–16.
[2] A.M. Azad, S. Larose, S.A. Akbar, J. Mater. Sci. 29 (1994) 4135–4151.
[3] N.M. Sammes, G.A. Tompsett, H. Nafe, F. Aldinger, J. Eur. Ceram. Soc. 19 (1999) 1801–1826.
[4] J.W. Fergus, J. Power Sources 162 (2006) 30–40.
[5] S.W. Zha, C.R. Xia, G.Y. Meng, J. Power Sources 115 (2003) 44–48.
[6] D.J. Kim, J. Am. Ceram. Soc. 72 (8) (1989) 1415–1421.
[7] S.J. Hong, A.V. Virkar, J. Am. Ceram. Soc. 78 (2) (1995) 433–439.
[8] J.G. Li, T. Ikegami, T. Mori, T. Wada, Chem. Mater. 13 (2001) 2921–2927.
[9] D.P. Fagg, J.C.C. Abrantes, D. Pérez-Coll, P. Núñez, V.V. Kharton, J.R. Frade, Electrochim. Acta 48 (2003) 1023–1029.
[10] D.J. Kim, J. Am. Ceram. Soc. 72 (1989) 1415–1421.
[11] R.D. Shannon, C.T. Prewitt, Acta Crystallogr. A 32 (1976) 751–767.
[12] B.C.H. Steele, Solid State Ionics 129 (2000) 95–110.
[13] W. Huang, P. Shuk, M. Greenblatt, Chem. Mater. 9 (1997) 2240–2245.
[14] W. Huang, P. Shuk, M. Greenblatt, Solid State Ionics 113–115 (1998) 305–310.
[15] S. Dikmen, P. Shuk, M. Greenblatt, Solid State Ionics 112 (1998) 299–307.
[16] S. Dikmen, P. Shuk, M. Greenblatt, Solid State Ionics 126 (1999) 89–95.
[17] S. Dikmen, P. Shuk, M. Greenblatt, H. Gocmez, Solid State Sci. 4 (2002) 585–590.
[18] X.F. Guan, H. Zhou, Y. Wang, J. Zhang, J. Alloys Compd. 464 (2008) 310–316.
[19] F.Y. Wang, S. Chen, S. Cheng, Electrochem. Commun. 6 (2004) 743–746.
[20] F. Wang, S.Y. Chen, Q. Wang, S. Yu, S. Cheng, Catal. Today 97 (2004) 189–194.
[21] X.Q. Sha, Z. Lu, X.Q. Huang, J.P. Miao, L. Jia, X. Xin, W. Su, J. Alloys Compd. 424 (2006) 315–321.
[22] N. Kim, B. Kim, D. Lee, J. Power Sources 90 (2000) 139–143.
[23] S. Liping, H. Lihua, Z. Hui, L. Qiang, C. Pijolat, J. Power Sources 179 (2008) 96–100.
[24] Y.P. Fu, C.W. Tseng, P.C. Peng, J. Eur. Ceram. Soc. 28 (2008) 85–90.